Accelerated and Robust Computation of Time Domain Floquet Wave-Based Periodic Green's Functions for TD Integral Equations Applications

M. Saviz[1] and R. Faraji-Dana[2]

[1]School of Electrical and Computer Engineering
University of Tehran, Tehran, Iran
msaviz@ut.ac.ir

[2]Center of Excellence on Applied Electromagnetic Systems,
University of Tehran, Tehran, Iran
reza@ut.ac.ir

Abstract **–** A novel approach has been introduced to remedy the computational complexities of the recently introduced time domain periodic Green's functions in the 1D and 2D periodic case. Specifically, it has been shown that for a certain class of temporal basis functions, the computational cost of convolutions with temporal basis functions, which results in the band-limited GFs needed by most time domain integral equations solvers, can be considerably reduced, as compared to conventional methods that are currently in practice. It is also well known that the computational complexity of the Floquet-wave based Green's functions increases when the point of observation approaches a source. Robust forms have been obtained for both 1D and 2D periodic TDGFs for any source-observation distance, which are then further improved for high-efficiency numerical implementation.

Index Terms **–** Time Domain Integral equations, Green's Function, Periodic Structures, Efficient Algorithms.

I. INTRODUCTION

Periodic structures serve as useful models for many real-world problems including antenna arrays and Frequency-selective surfaces and promisingly fast formulations in this area have been recently reported [1-4]. Infinitely extended periodic arrays of sources are amenable to more elegant, and sometimes more convenient mathematical descriptions than those which are finite. In the area of integral equation techniques, and also with many other numerical methods, the "periodic" Green's function refers to the inclusion of the effects of all elements of an array at the observation point (located in the unit cell) in a unified Green's function. This reduces the numerical domain of the original periodic problem to the unit cell of the periodic array. The most straight-forward approach to compute such Green's functions (GF) is to directly sum up the contributions from all elements whose received amplitude at the unit cell is considered to be significant. This direct summation approach (DS) to obtaining such GFs is not computationally efficient, as the resulting series converges rather slowly. In the frequency domain (FD), extensive efforts have been devoted to the problem of finding fast and computationally efficient expressions of the periodic Green's functions and rather efficient implementations do exist. A good review of these can be found in [5]. Such periodic GFs can also be applied in solving finite arrays[6].

Submitted On: May 24, 2012
Accepted On: Aug. 22, 2012

In time domain (TD), analysis of periodic structures has been attempted in recent years [7], based on the TD equivalents of FD Floquet-wave Green's functions developed in [8-11], and further expanded in [12]. Although representations of periodic GFs based on TD-Floquet-wave series (FW) give a more natural approach to a periodic problem, and their corresponding expressions for TDGFs can provide for faster evaluation of impulsive Green's functions, their final implementation in time domain integral equations (TDIE) requires extra convolutions with temporal basis functions (TBFs) and requires special considerations near a source point. These issues greatly affect their speed and efficiency, and consequently, their practical application to TDIE. To the best knowledge of the authors, these aspects have not yet been comprehensively addressed. This paper reports findings related to these important, practical issues.

To have the material needed for further steps, it is necessary to briefly review the Floquet-based Green's functions in section II. Section III introduces the fast convolution technique for periodic time domain GFs with a well-known class of temporal basis functions. Section IV discusses the numerical difficulties encountered when evaluating 1D periodic Floquet-wave GFs close to a source-point, and introduces a novel method to mitigate these effects based on source extraction for the 1D periodic case. We then verify the proposed method through a numerical example. Section V investigates source-proximity improvements for the 2D periodic case, proposes several ways to accelerate the computation of the TDGFs, and verifies the results by numerical examples. Section VI summarizes the contributions of this paper.

II. Preliminaries

Consider a 1D-periodic, infinite, sequentially-excited array of point sources lying along the x-axis, as in Fig. 1.

Considering the surrounding environment of the elements to be free space, and the sequential inter-element delay to be proportional to inter-element spacing X through a factor $\eta = \cos\theta_x$, the sum of potentials contributed by all elements at an observation point (x,y,z) is

$$\tilde{G}(\vec{r},\omega) = \sum_{m=-\infty}^{\infty} \frac{e^{-jmkX\eta} e^{-jkR_m}}{4\pi R_m}, \tag{1}$$

$$G(\vec{r},t) = \sum_{m=-\infty}^{\infty} \frac{\delta\left(t - \frac{R_m}{c} - \frac{m\eta X}{c}\right)}{4\pi R_m}, \tag{2}$$

where $R_m = \sqrt{(x-mX)^2 + \rho^2}$ and $\rho = \sqrt{y^2+z^2}$, and $k = \omega/c$. It has been assumed, in accordance with previous work [8], that the sources are impulsively excited.

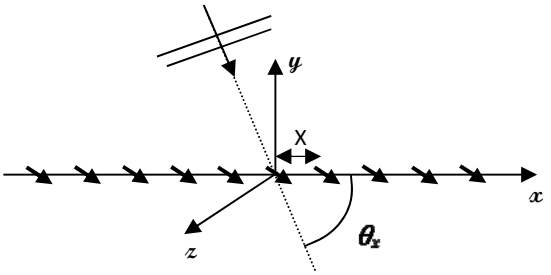

Fig. 1. Linear periodic array of dipole point sources. The plane wave shows one possible way of exciting this array by an inter-element delay of $\eta X = X\cos\theta_x$.

As the denominators in (1) and (2) might suggest, these series converge slowly. Moreover, in many problems, the three dimensional spatial domain of evaluation in (1,2) makes a pre-storage and interpolation approach to their fast evaluation rather expensive and impractical. For this reason, alternative expressions or approximations for these functions are sought. To elaborate the approach in [8], consider the discrete line array of point sources. In frequency domain, one can describe this periodic source structure by (3);

$$\tilde{J}(\omega) = \sum_{m=-\infty}^{\infty} \delta(x' - mX) e^{-jkm\eta X}, \tag{3}$$

which can describe any of the spatial orientations. we can use the Poisson's summation formula $\sum_{m=-\infty}^{\infty} \delta(x'-mX) = X^{-1} \sum_{q=-\infty}^{\infty} \exp(-j2\pi q x'/X)$ to obtain an alternative expression for the sources as:

$$\tilde{J}(\omega) = \sum_{m=-\infty}^{\infty} \delta(x'-mX) e^{-jk\eta x'} = \frac{1}{X} \sum_{q=-\infty}^{\infty} e^{-jk_{xq}x'}, \tag{4a}$$

in which

$$k_{xq}(k) = k\eta + \alpha_q;\ \ \alpha_q = \frac{2\pi q}{X},\ \ q = 0, \pm 1, \pm 2, \ldots \quad (4b)$$

Equation (4) expresses the discrete array of point sources as an infinite summation over smooth linear sources. Correspondingly, the Green's function can be stated in terms of the Green's functions for linear sources; which gives (in frequency domain) [8]

$$\tilde{G}^{FW}(\vec{r}, \omega) = \sum_{q=-\infty}^{\infty} \frac{e^{-jk_{xq}x}}{4jX} H_0^{(2)}(k_{\rho q}\rho), \quad (5)$$

in which $k_{\rho q}(k) = \sqrt{k^2 - k_{xq}{}^2}$. Each of the summands in (5) comprises a Floquet mode. Note that these modes are evanescent away from the linear axis whenever $|k| < |k_{xq}|$, under which the argument of the Hankel function becomes imaginary ($\mathrm{Im}[k_{\rho q}] \le 0$ is assumed, in order to satisfy the radiation condition as $\rho \to +\infty$). The second and fifth FD Floquet-waves are depicted in Fig. 2 for an example with $x = y = 0.25m, z = 0$ in an array with $X = 1m$ and $\eta = 0$. The important cut-off property of these modes before a certain frequency can be readily observed. This implies that for a certain frequency, the summation of a limited number of modes can reconstruct the GF with sufficient accuracy. This is verified in Fig. 3, where the summation of Floquet modes of $|q| \le 2$ has been shown to suffice for an entire frequency region nearly up to the cut-off frequency of the next higher mode.

It can be anticipated that by performing an inverse Fourier transform of the GF in (5), the desirable convergence properties of (5) will carry over to the time domain. Doing so, one arrives at the time domain Floquet modes, with the current modes given by (6) and the corresponding TD Green's functions in (7).

$$J(t) = \frac{1}{X} \sum_{q=-\infty}^{\infty} e^{-j\alpha_q x'} \delta\left(t - \frac{\eta x'}{c}\right). \quad (6)$$

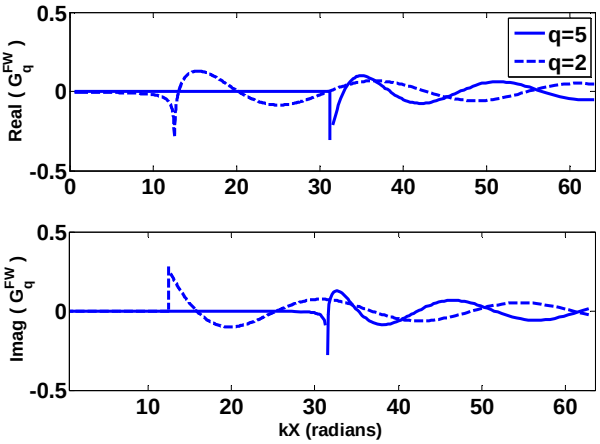

Fig. 2. The 2'nd and 5'th FD Floquet waves observed at $x = y = 0.25m, z = 0$ for an array with $X = 1m$ and $\eta = 0$. The infinity-spikes observed are inherent to periodic Green's functions.

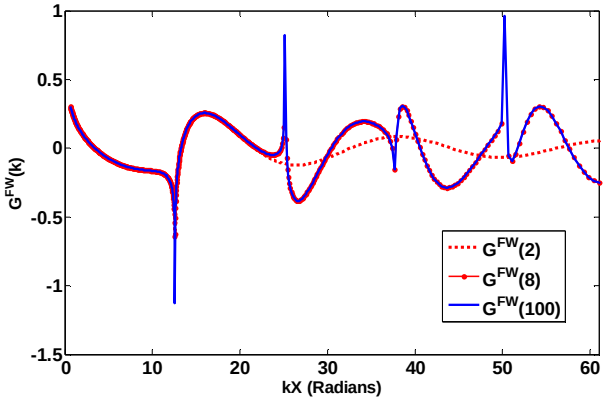

Fig. 3. Comparison between the Floquet GF (5) up to a certain mode number (given in parentheses) and actual (direct summation, equation (1) with 100 terms) observed at $x = y = 0.25m, z = 0$ for an array with $X = 1m$ and $\eta = 0$. Only the real part is shown. The imaginary part shows similar behaviour.

Each TD Floquet current can be interpreted as a traveling impulse excitation along the x-axis, with an x-dependent harmonic amplitude. The resulting TD Green's function can be shown to be, in its most computationally efficient representation [8]:

$$G^{FW}(\vec{r},t) = G_{+}^{FW}(\vec{r},t) + G_{-}^{FW}(\vec{r},t) = \sum_{q=0}^{Q} \varepsilon_q \frac{\cos(\alpha_q x'_{+}(t)) + \cos(\alpha_q x'_{-}(t))}{2\pi X\sqrt{\tau^2 - \tau_0^2}} U(\tau - \tau_0), \quad (7a)$$

where $\varepsilon_q = 1/2$ for $q=0$ and $\varepsilon_q = 1$ otherwise. $U(\tau)$ is the Heaviside function, $\tau = t - \eta x/c$ and

$$x'_{\pm}(t) = x - \frac{c}{1-\eta^2}\left(\eta\tau \pm \sqrt{\tau^2 - \tau_0^2}\right), \quad (7b)$$

$$\tau_0 = \sqrt{1-\eta^2}\,\frac{\rho}{c} = t_0 - \eta\frac{x}{c}. \quad (7c)$$

The physical interpretation of (7) is fairly simple: the instantaneous signal received at the observation point $\vec{r}$ at a certain time t has been contributed by impulsive current excitations at two points $x'_{\pm}$ on the axis; whose sequential excitation and propagation delays have been appropriate for reception at $\vec{r}$ at the time t. These points are time-dependent and are displaced farther away with time.

Of computational significance is the fact that t_0 is independent of q; the mode number. Consequently received signals from all modes begin at the same time t_0 which is, however, dependent on the observation point. Several TD Floquet-wave modes are shown in Fig. 4. It is seen that all modes begin with a sharp variation at t_0 but can be described by different late-time oscillation frequencies (obtained for large t in 7) of

$$\omega_{\pm}^{FWq} = 2\pi\left(\frac{q}{T_X}\right)\left(\frac{1}{1\pm\eta}\right), \quad (8)$$

where we denote the characteristic time scale of the periodic lattice by $T_X = X/c$.

Because the TD Green's function in (2) has been obtained assuming impulsive excitation of point sources, for most numerical applications of Floquet-modes, these have to be convolved with certain TBFs (temporal basis functions or pulse shapes) in order to limit their bandwidth to that appropriate for TDIE simulations (i.e. the band-limited TDGF). The number of Floquet modes required can be estimated by those that have their cut-off below the effective bandwidth of the TBF. Based on the discussion following (5) and approximating the TBF bandwidth by $\Delta\omega = 2\pi/T$, where T is the solver time step, the number of modes that contribute as propagating in the desired bandwidth can be derived as:

$$q < Q = \frac{T_X}{T}\max\left[(1-\eta),(1+\eta)\right]. \quad (9)$$

The number of modes for the case of normal incidence is $Q = T_X/T$. In many problems a choice of $T = 0.1T_X$ can be reasonable for TDIE solutions.

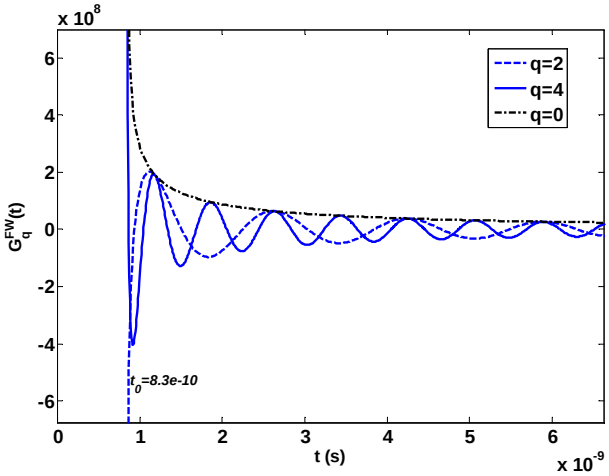

Fig. 4. Time domain Floquet modes from equation (6), for an array with X=1m and $\eta = 0$.

It can be verified from the number of terms needed to produce agreement with the actual GF in Fig. 5a, that the TD Green's function in (7) has indeed inherited the desirable convergence properties of their FD counterpart (5). Here a QB-spline basis function with $T = T_X$ has been used as the temporal basis functions, for which mode indices as low as $Q = 1$ should be sufficient according to (9). Other parameters in Fig. 5a are similar to the previous FD example.

In spite of the efficient number of required modes, the necessary convolutions $G_q^{FW}(t) * g(t)$ usually have to be performed numerically at a temporal discretization of about $\Delta t < 0.1\min\left[T, 2\pi/Max(\omega_{FW})\right]$. This is typically more than an order of magnitude smaller than the time step T in a typical TDIE solver (e.g. based on the marching-on-in-time method) which needs the TDGF to be obtained at integer multiples of T only. This makes the convolution time-consuming. Indeed, for short simulation times T_{sim}, the higher

resolution in time that is required to perform the convolution with accuracy, increases the total computational cost of the Floquet-based approach beyond that of direct summation of element Green's functions at integer multiples of T(see Fig. 9). We shall assume from now on that Δt is chosen so that T is an integer multiple of Δt .

It is usual in TDIE solvers such as MoT to use temporal basis functions which have a temporal support of one to several T. The ratio $N_b = T/\Delta t$ will be useful in later discussions.

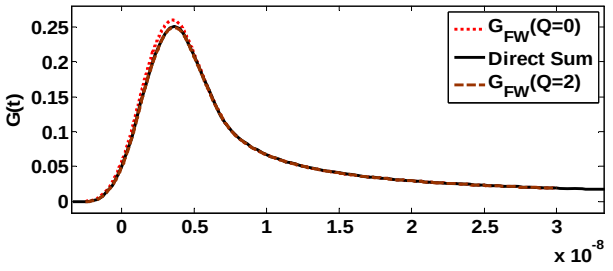

(a)

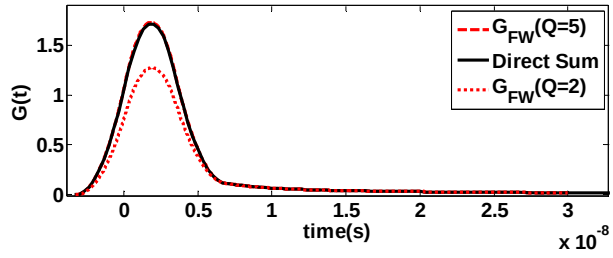

(b)

Fig. 5. Band-limited Time domain Green's functions obtained by direct summation (equation 2) and Floquet-waves (11) for a. $x = y = 0.25m, z = 0$ and for b. $x = y = 0.025m, z = 0$.

It is also well known when using the TDGFs of (7) that a higher number of modes are needed when the point of observation approaches a source point (e.g. the origin in (2)). This can be seen in Fig. 5b where the point of observation has been moved to $x = y = 0.025m, z = 0$ for the same array of the previous example. The reason for this can be traced back to the FD Floquet GFs in (5). At low values of ρ , the evanescent tails of the Hankel functions become more and more pronounced below their cut-off frequencies, and at $\rho = 0$ a smooth, constant value can be contributed by these modes in the bandwidth of interest. Consequently the number of higher order Floquet modes required to reproduce the TDGF grows enormously as $\rho \to 0$, and a computation using Floquet series would be far from efficient. This does not come as a surprise, as it is generally known that modal expansions of GFs perform best for far-fields and direct summations perform best for near-fields. This problem affects the accuracy of self-patch terms in the MoT coefficients matrix, and can trigger instabilities in the TDIE solution.

As the 2D periodic problem has the same essential features observed in the above discussion of the 1D periodic case, we do not present an introduction for them here. We refer the interested reader to [9,10] for a detailed discussion. After considering an accelerated method of convolution in section 3, section 4 and 5 provide modifications of expressions like (7) to overcome the accuracy problem while maintaining computational efficiency, for the 1D and 2D periodic problems respectively. To facilitate the following discussion, many of the related symbols and parameters have been defined and described in Table 1, with their typical values. Other symbols will be defined when they are first used in the text.

Table 1: Symbols that are repeatedly used throughout the paper.

Symbol	Description	Typical Value
T	Solver *time step*. The time support of the temporal basis function (TBF) can be one to several (denoted n_{TBF}) *time steps.*	For min. excitation wavelength of $O(X)$, $T \sim 0.1(X/c_0)$.
T_{sim}	The time limit up to which (starting at t=0) the TDGF has to be computed for a certain TD problem.	
N_{sim}	The length of the computer vector of time samples, for which the GF has to be computed. $N_{sim} = \lceil T_{sim} / T \rceil$.	> 100
Δt	Because of the numerical convolution of the Floquet-modes with the TBF, the floquet modes have to be computed at a higher resolution $\Delta t < T$.	$\Delta t \sim 0.1T$, usually chosen so that T is an integer multiple of Δt .
N_b	$N_b = \lceil T / \Delta t \rceil$, also the length of the MA filter in section 3.	*10-50*

III. Efficient computation of convolutions with TD Green's functions

Stable TDIE formulations have been reported using the B-spline family of temporal basis functions and marching in time (MoT) solvers[13,14]. B-spline pulses are piecewise-polynomial functions and provide compact support in time, which ensures the sparsity of MoT matrices at later time steps. A B-spline pulse of order m can be built through the following desirable property[15]:

$$b_0(t) = rect(\frac{t}{T})$$
$$b_m(t) = \frac{1}{T} b_0(t) * b_{m-1}(t), \quad m \in \mathbb{N} = \{1,2,...\}. \qquad (10)$$

The *zero'th order* B-spline is the simple rectangular pulse of width *T*. The first order can be obtained by convolving the rectangular pulse function by itself and dividing by *T*, which gives the rather common roof-top, or triangular basis function. Convolving once more with the rectangular pulse function results in the second order or Quadratic B-spline (QB-spline) function which has been used in the time domain integral equations developed in[13,15]. As noted in [13] the time derivative of the QB-spline basis functions are continuous, which makes them suitable for EFIE formulations, where time derivatives of the basis functions appear. We note that to construct the TBFs, the QB-spline and higher B-splines are used with positive time shifts so that the TBF equals zero for $t < -T$. This is important for a causal TDIE solver such as MoT.

The property in (8) can be used to efficiently compute the convolution with B-splines. To elaborate, consider the convolution of a QB-spline basis $b_2(t)$ with $G(\vec{r},t)$ of (7). We shall denote the band-limited TDGFs by $S_m(t)$, where m shows the order of the basis function used. Consider rewriting the convolution as:

$$S_2(t) = G(t) * b_2(t) = \frac{1}{T^2} G(t) * \left[b_0(t) * b_0(t) * b_0(t) \right]$$
$$= \frac{1}{T^2} \left[G(t) * b_0(t) \right] * b_0(t) * b_0(t) \qquad (11)$$

We shall first concentrate on convolving $b_0(t)$ namely:

$$S_0(t) = G(t) * b_0(t) = \int_{-\infty}^{\infty} G(\tau) b_0(t-\tau) d\tau. \qquad (12)$$

Computer implementation of (12) requires discretization in time. Assuming a sampling interval of Δt we will denote the discrete waveform of the signal $S(t)$ by $S[n] = S(n\Delta t)$, and the computer vectors which can only have positive integers as indices will be denoted by the bold caharacter **S**(j). Every vector starts with the first nonzero sample of the corresponding signal. Thus **G**(1) corresponds to $G(t_0)$ and **b**(1) corresponds to $b_0(-T/2)$. Keeping these in mind, we shall only use the computer vectors in the following to facilitate the discussion. The convolution is:

$$\mathbf{S}_0(i) = \sum_j \mathbf{G}(j) \mathbf{b}_0(i-j+1). \qquad (13)$$

There are only $N_b = T/\Delta t$ nonzero samples in $\mathbf{b_0}$. The constant, unity amplitude of $\mathbf{b_0}$ in this range allows to avoid the multiplication step in the process of convolution. Computing the convolution therefore reduces to finding the sum of N_b elements of **G** at each step *i*. This provides for a "Moving Average" (MA) Interpretation of the convolution in (13). This procedure would cost half that of direct convolution, because it avoids one multiplication for every summation in (13). Nevertheless, the procedure can be done still much faster. It is known, mostly among the image-processing community, that two-dimensional moving averages can be computed with high efficiency "Box-filtering" Techniques [16]. We show the one-dimensional application of the idea to the problem in hand. Suppose the moving average has been computed for the first N_b samples of the signal G. The moving average window then slides one sample to the right to compute the next N_b -sum. However, It suffices at this step to subtract one of the previous samples (i.e. the earliest), and add one new sample (Fig. 6) to the output of the previous step. This involves only two operations per step instead of N_b in a conventional MA.

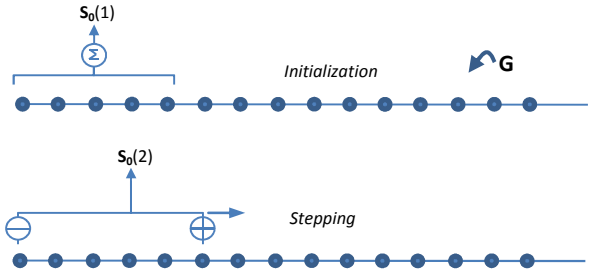

Fig. 6. The convolution with b_0 as a moving average with higher efficiency.

From a programing point of view, in the MA method of Fig. 6, **G** has to be padded with $N_b - 1$ zeros at its beginning. In this way the first element of $\mathbf{S_0}$ will correspond to $S_0(t_0 - T/2)$, and through the convolution in (12), $S_0(t)$ is indeed known to be nonzero only after $t = t_0 - T/2$. Considering N_G to be the number of elements in **G,** The whole process has a computational complexity of $2N_G$ only.

An efficient sample algorithm for one iteration is shown below (all time samples are computed simultaneously by vectorized programming).

1. Compute the difference for all time samples with the ones shifted by N_b samples:

```
PGF(Nb+1:end)= PGF(Nb+1:end)-PGF(1:end-Nb)
```

2. Compute the cumulative summation:

```
PGF=cumsum(PGF),
```

where `cumsum` stands for cumulative summation, i.e. a vector that has the same length as the input whose elements are obtained by cumulatively adding the input elements, with its first element being equal to the first of the input. In order to compute the desired convolution with $b_2(t)$, the same process has to be iterated three times according to (11) and the final result multiplied by a constant $\Delta t^3 T^{-2}$. The whole computational complexity of this method is then only $7N_G$. The first element of $\mathbf{S_2}$ obtained after three iterations corresponds to $S_2(t_0 - 3T/2)$, which is indeed the starting time for $S_2(t)$. We shall note that for a shifted QB-spline basis function [13,15] which starts at $t = -T$, the above procedure remains the same, and the first element of $\mathbf{S_2}$ obtained after three iterations is simply assigned to $S_2(t_0 - T)$. Furthermore, the first time-deriviative of the TDGF can be obtained by simply omitting the final cumulative sum.

IV. COMPUTATION OF THE TD GREEN'S FUNCTION CLOSE TO A SOURCE: 1D PERIODICITY

A. Formulation

Although the procedure described above can provide for efficient computation of TDGF, at observation points close to a source, the number of Floquet modes that have to be considered for an accurate reconstruction of the TDGF increases beyond those that are considered as propagating in the TBF bandwidth. The problem has been already discussed in section 2. It would be of advantage to find a robust procedure for the evaluation of the TDGF, which overcomes the source-proximity problem and can still benefit from the fast computational techniques of the previous section.

We see from Fig. 5 that the discrepancy is an early-time phenomenon. At these times the TDGF values can be attributed to the signal received from the nearby sources. Because in a TDIE we only have observation points in the unit interval of the periodic array, i.e. $x \in (0, X)$, we can extract the two near-by sources on both sides of the unit interval and add their contribution separately. Using (2) as our starting point, we have:

$$\begin{aligned} S_{1D}(\vec{r},t) = &\sum_{n=-\infty}^{-1} \frac{g\left(t - \frac{R_n}{c} + \frac{\eta X}{c}\right)}{4\pi R_{-1}} \\ &+ \frac{g\left(t - \frac{R_0}{c}\right)}{4\pi R_0} + \frac{g\left(t - \frac{R_1}{c} - \frac{\eta X}{c}\right)}{4\pi R_1} \\ &+ \sum_{n=2}^{+\infty} \frac{g\left(t - \frac{R_n}{c} - \frac{2\eta X}{c}\right)}{4\pi R_2}. \end{aligned} \tag{14}$$

For the rest of the array, we then use the Floquet modes of two semi-infinite linear periodic arrays. Details of deriving these modes are given in [9]. A semi-infinite linear array lying over $[0, +\infty)$ has the truncated GF G^T given in (13):

$$\begin{aligned} G^T(\vec{r},t) = &\frac{\delta\left(t - \frac{R_0}{c}\right)}{8\pi R_0} \\ &+ G_-^{FW} U\left(x'_+(t)\right) \\ &+ G_+^{FW} U\left(x'_-(t)\right), \end{aligned} \tag{15}$$

Where G_+^{FW}, G_-^{FW} come from the TDGF of the infinite array as in (7), corresponding to terms with x'_+, x'_- respectively. The first term in (15) is the spatial TDGF of the single element at the truncated end, divided by two. We rewrite this for the two series in (14) and simplify to arrive at (16), which is written in its most computationally compact form:

$$\begin{aligned} S_{1D}(\vec{r},t) = &\frac{g\left(t - \frac{R_0}{c}\right)}{4\pi R_0} + \frac{g\left(t - \frac{R_1}{c} - \frac{\eta X}{c}\right)}{4\pi R_1} \\ &+ \frac{g\left(t - \frac{R_{-1}}{c} + \frac{\eta X}{c}\right)}{8\pi R_{-1}} + \frac{g\left(t - \frac{R_2}{c} - \frac{2\eta X}{c}\right)}{8\pi R_2} \\ &+ G^{RE} * g(t), \end{aligned} \tag{16a}$$

where

$$\begin{aligned} G^{RE} = &G_+^{FW} . \left[1 - U\left(x'_+(t) + 1\right) \cdot U\left(2 - x'_+(t)\right)\right] \\ &+ G_-^{FW} . \left[1 - U\left(x'_-(t) + 1\right) \cdot U\left(2 - x'_-(t)\right)\right] \end{aligned} \tag{16b}$$

and $U(\cdot)$ is the Heaviside function. The terms in brackets in (16b) effectively extinguish the Floquet-mode contributions from the region between the point sources corresponding to m= -1 and m=2. The result in (16) is quite general and not limited to using B-spline functions for g(t). Using (16), High accuracy reconstruction of the final band-limited TDGF can be obtained at both early and late times without including higher order modes.

For B-spline functions, the implementation of convolutions in (16) can benefit from the simplification and convolution-acceleration technique discussed in the previous section. Furthermore we can incorporate the four leading terms in (16) in the convolution process, by considering $g(t-a)=\delta(t-a)*g(t)$. For computer implementation, we insert four samples in the computer vector corresponding to G^{RE} prior to convolution with $g(t)$. These samples correspond to discrete versions of the Dirac delta function, whose amplitudes and locations are shown in Table 2 in order to facilitate the reproduction of our results.

By the process of moving averages, these will automatically give rise to the four direct terms, thereby avoiding programming calls to evaluate $g(t)$ altogether. The desired values of the TDGF for a TDIE solver which runs at steps of T are then obtained by down-sampling by N_b.

Table 2: Locations and amplitudes of the four discrete impulse functions to numerically generate the first four terms in (16)

Corresponding term in (16)	Sample Amplitude	Location[a]
$\dfrac{g\left(t-\frac{R_0}{c}\right)}{4\pi R_0}$	$\dfrac{\Delta t^{-1}}{4\pi R_0}$	$\left\lceil \dfrac{R_0}{c}-t_0 \right\rceil$
$\dfrac{g\left(t-\frac{R_1}{c}-\frac{\eta X}{c}\right)}{4\pi R1}$	$\dfrac{\Delta t^{-1}}{4\pi R_1}$	$\left\lceil \dfrac{R_1}{c}+\dfrac{\eta X}{c}-t_0 \right\rceil$
$\dfrac{g\left(t-\frac{R_2}{c}-\frac{2\eta X}{c}\right)}{4\pi R_2}$	$\dfrac{\Delta t^{-1}}{4\pi R_2}$	$\left\lceil \dfrac{R_2}{c}+\dfrac{2\eta X}{c}-t_0 \right\rceil$
$\dfrac{g\left(t-\frac{R_{-1}}{c}+\frac{\eta X}{c}\right)}{4\pi R_{-1}}$	$\dfrac{\Delta t^{-1}}{4\pi R_{-1}}$	$\left\lceil \dfrac{R_{-1}}{c}-\dfrac{\eta X}{c}-t_0 \right\rceil$

[a]The element location assumes the first element of the computer vector $\mathbf{G}^{\mathbf{RE}}$ to correspond to t_0.

B. Numerical example

We shall now consider an example where the observation point is extremely close to the source, i.e. $x=y=0.00025m, z=0$ in an array with $X=1m$ and $\eta=0$ and by choosing $T=0.1T_X$. The results for this example are shown in Fig. 8. The accuracy of (16) has been compared against the previous pure-Floquet-modes approach. The number of modes in both cases are the same, and are chosen as low as indicated by (9). In addition to the capability of accurate reconstruction, the formula in (16) is free from the Gibbs-phenomenon at early times. It smoothly joins the Floquet-modes results. at later times, where they are more accurate.

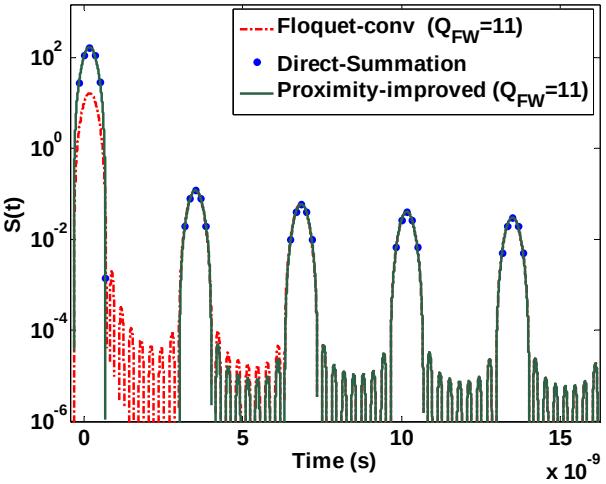

Fig. 8. Comparison of the Floquet-convolution approach with the proximity- improved formula in (16). As the amplitude of the first peak is at least two orders of magnitude higher than others near the source point, a logarithmic scale has been chosen to observe the whole-range function behaviour.

In Fig. 9 we compare the performance of several methods of computing the convolution in the proximity-improved function $S_{1D}(\vec{r},t)$ in (16). This is done by implementing all methods in MATLAB programming environment and running the computations for increasing simulation times T_{sim}. In this way the computation load on each method is increased by increasing the number of required time samples (vector length), while keeping a constant $\Delta t=0.01\min\left[T,\,2\pi/\max(\omega_{FW})\right]$ for accurate numerical convolutions. The temporal basis functions are QB-spline pulses and for each value of T_{sim}, the total computer time required to perform the GF calculation for t=-T to T_{sim} is taken

as an approximate indicator of computational cost.(Considering the faster implementation of built-in functions, this might not be a fair criterion, i.e. underestimating the proposed method. Nevertheless, we expect to have at least a correct qualitative comparison.)

Convolution and FFt-based Floquet refer to evaluating the first four terms of (16) directly and using either direct convolution or FFt-based convolution to evaluate the fifth term. Floquet-MA refers to implementing Table 1 and using the MA convolution scheme. To perform a fair comparison, we note that direct summation (DS) needs to evaluate no more than $M_{DS} = T_{sim} / T_X + 1$ individual elements at both sides of the origin, as the contribution from other elements of the lattice arrive later than $t = T_{sim}$. furthermore, in accordance with a real TDIE scenario, only samples at integer multiples of T are required, which amount to $N_{sim} = T_{sim} / T$ time points. These indicate that direct summation GFs can have low computational time for small simulation times. The rise in Computation time is, however, proportional to $M_{DS} N_{sim}$, which is $O\left(N_{sim}{}^2\right)$, as evidenced by the corresponding slope in Fig. 9. Direct numerical convolution will have a computational cost of at least $2N_G N_b$, which is $O\left(N_{sim}\right)$. Indirectly computing the convolution by means of three times Fast Fourier Transforms (two times FFT, and one inverse FFT) all of equal lengths N_G will result in a cost of $O(N_{sim} \log(N_{sim}))$ [17], and might not necessarily be more efficient than direct convolution for all N_{sim}. Finally, the proposed method, which relies on a moving-average (MA) scheme and needs no evaluation of g(t), has a computational cost of $7N_G$ only and has considerably better efficiency. In Fig. 9, all Floquet-based computation times also include the time to compute the Q+1 Floquet-modes, prior to convolution.

V. COMPUTATION OF THE TD GREEN'S FUNCTION CLOSE TO A SOURCE: 2D PERIODICITY

This section extends the previous investigation to doubly periodic GFs and discusses some specific points for more efficient programming. To preserve notational simplicity, we reuse some of the symbols from the previous sections with new meanings specific to the 2D periodic GF.

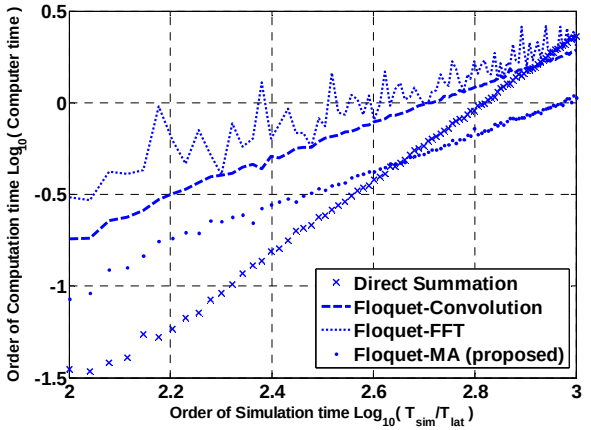

Fig. 9. Comparison of the computation times for the proposed method with several other approaches.

A. Formulation

For a sequentially excited doubly-periodic array of point-dipole elements, which has unit cell dimensions of X and Y as shown in Fig. 10, one can readily write the field at an observation point (x,y,z) as a summation over all elements in Frequency domain (FD) and time domain (TD):

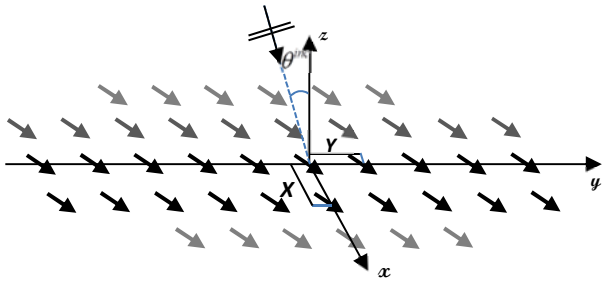

Fig. 10. Schematic description of the infinite doubly periodic array. The hypothetical plane wave shows one possible way to excite this array by an inter-element delay of $\eta \hat{u}^{inc} = \eta \cos\varphi^{inc} \hat{x} + \eta \sin\varphi^{inc} \hat{y}$, where $\eta = \sin\theta^{inc}$

$$\tilde{G}(\vec{r},\omega) = \sum_{m=-\infty}^{\infty} \sum_{n=-\infty}^{\infty} \frac{\exp\left[-jk\left(R_{mn} + mX\eta\cos\varphi^{inc} + nY\eta\sin\varphi^{inc}\right)\right]}{4\pi R_{mn}} \tag{17}$$

$$G(\vec{r},t) = \sum_{m=-\infty}^{+\infty} \sum_{n=-\infty}^{+\infty} \frac{\delta\left(t - \frac{R_{mn}}{c} - \eta\frac{mX\cos\varphi^{inc} + nY\sin\varphi^{inc}}{c}\right)}{4\pi R_{mn}} \tag{18}$$

where $R_{mn} = \sqrt{(x - mX)^2 + (y - nY)^2 + z^2}$ and $k = \omega/c$, and η, φ^{inc} and θ^{inc} have been explained

in Fig. 1. We note that the symbol η is reused form the previous section and $\eta = \sin\theta^{inc}$. It has been assumed in (18), in accordance with previous work [10], that the sources are impulsively excited. Direct computation of (17) and (18) is even more costly than in the 1D case (considering that the minimum number of elements now varies with the square of the simulation time). As in the 1D periodic case, for both FD and TD, the Floquet-wave representations can very efficiently reconstruct the TDGF (18); in most cases requiring up to only a few tens of modes to converge. The 2D periodic TD modes are given in (3) as:

$$G^{FW}(\vec{\rho},z,t) = \sum_{p=0}^{\infty}\sum_{q=-\infty}^{\infty} \varepsilon_p \frac{c\cos\left[\alpha_{pq}.(x\hat{x}+y\hat{y})-\bar{\omega}_{pq}\tau\right]}{XY\sqrt{1-\eta^2}} \times J_0\left(\tilde{\omega}_{pq}\sqrt{\tau^2-\tau_0^2}\right)U(\tau-\tau_0), \quad (19a)$$

where $\varepsilon_p = 1$ for $p \neq 0$ and $\varepsilon_p = 1/2$ for $p = 0$, $J_0(\cdot)$ denotes the zero'th order Bessel function and $U(\cdot)$ the Heaviside function, and the parameters are[10]:

$$\begin{aligned} &\eta = \sin\theta^{inc} \quad , \quad \hat{u}^{inc} = \cos\varphi^{inc}\hat{x} + \sin\varphi^{inc}\hat{y} \\ &\alpha_{pq} = \frac{2\pi p}{X}\hat{x} + \frac{2\pi q}{Y}\hat{y} \\ &\bar{\omega}_{pq} = \frac{\eta c}{1-\eta^2}\hat{u}^{inc}\cdot\alpha_{pq} \\ &\tilde{\omega}_{pq} = \sqrt{\bar{\omega}_{pq}{}^2 + \alpha_{pq}{}^2 c^2/1-\eta^2} \\ &\tau = t - \frac{\eta}{c}\hat{u}^{inc}\cdot(x\hat{x}+y\hat{y}) \\ &\tau_0 = \frac{\sqrt{1-\eta^2}}{c}z, \end{aligned} \quad (19b)$$

and it has to be reminded that to produce the band-limited GFs that are necessary in the implementation of TD integral equation solvers, the TDGF in (19) has to be convolved with a TBF (denoted $g(t)$), which we consider to have a bandwidth of approximately T^{-1}, where T is the solver time step. The efficiency of (19) can be understood by a glance at Fig. 11, where the reconstruction process is shown in both time and frequency domains. It is seen that away from the x-y plane, the evanescent character of higher modes in FD below $f=T^{-1}$ enables a limited number of modes to reproduce the band-limited TDGF. Nevertheless, as $|z| \to 0$, Like the 1D case, it is the early time of the TDGF that is affected. For a 2D periodic TDGF, this is more rigorously shown in [11; Appendix].

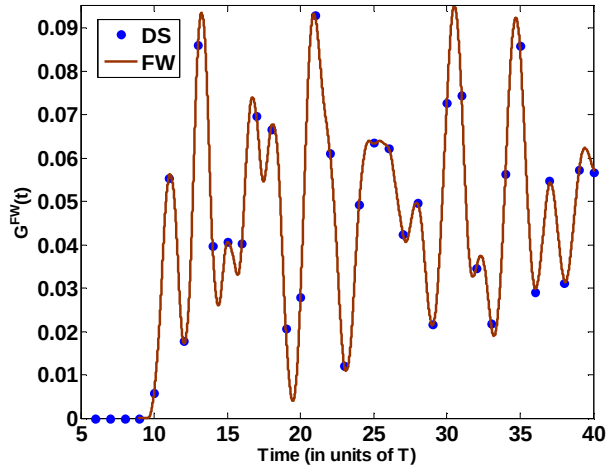

(a)

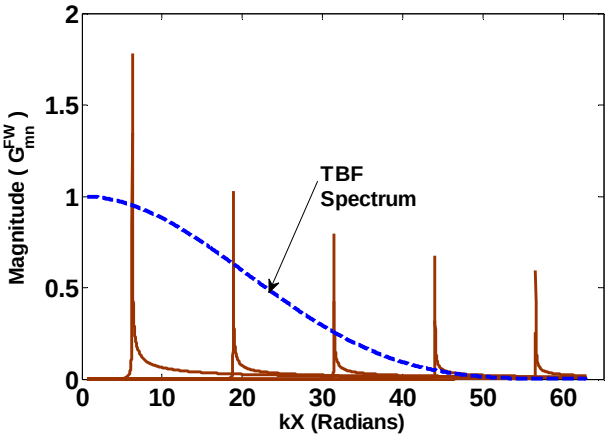

(b)

Fig. 11. (a) The 2D periodic TDGF for an example with $x = y = 0.25m, z = 1$ in an array with $X = Y = 1m$ and $\eta = 0$ where we have chosen $T = 0.1X/c_0$ for the TBF. Only modes with $|p|,|q| \le 10$ have been used. (b) the frequency domain description for the same example shows a limited number of modes being "selected" by the TBF spectrum. The FD modes shown correspond to $p = 0, q = 1,3,5,7,9$.

On the other hand, direct summation is most efficient for early times, because at early times one

can exclude from the summation in (18), all the element signals that have not yet arrived at the observation point (The observation point resides in the unit cell). Consequently, as with the 1D periodic GF, we seek a combination that uses direct summations at early times and Floquet-mode GFs at later times. However, unlike the 1D case, it might be easier here to separate the two methods in time, rather than in space. In [7], it has been suggested to separate the very early-time and compute it directly, and treat the later times with Floquet-modes. The following approach for 2D periodic GFs uses a similar technique in combining DS and Floquet-series. Additionally, we treat the TDGF explicitly, and optimize its computational procedure to arrive at a formulation which is accurate, and still more efficient computationally from either of the DS, or FW formulations.

A separation of the two methods in time requires defining a transition time T_{trans}. The simulation time T_{sim} is then divided into two parts, namely $0<t< T_{\text{trans}}$, and $T_{trans}<t<T_{sim}$. For the first part, the evaluation of the TDGF is done using direct summation in (18) with a limited number of elements determined by T_{trans}. The remaining time points after and including T_{trans} can be computed by Floquet-series. We can thus write:

$$S_{2D}\left(\vec{r}, t < T_{trans}\right) = \sum_{m=-M}^{+M}\sum_{n=-N}^{+N} \frac{g\left(t_{DS} - \frac{R_{mn}}{c} - \eta\frac{mX\cos\varphi^{inc} + nY\sin\varphi^{inc}}{c}\right)}{4\pi R_{mn}}$$

$$S_{2D}\left(\vec{r}, t \geq T_{trans}\right) = \left\{\sum_{p=0}^{P}\sum_{q=-Q}^{Q}\varepsilon_p \frac{c\cos\left[\alpha_{pq}.\left(x\hat{x}+y\hat{y}\right) - \bar{\omega}_{pq}\tau_{trunc}\right]}{2XY\sqrt{1-\eta^2}} \times J_0\left(\tilde{\omega}_{pq}\sqrt{{\tau_{trunc}}^2 - \tau_0^2}\right)\right\} * g(t), \quad \text{(20a)}$$

where

$$t_{DS} = jT, \quad j = 0,1,...,N_{trans}-1.$$
$$N_{trans} = T_{trans}/T.$$
$$M = \left\lceil \frac{T_{trans}}{X/c} \right\rceil + 1,\ N = \left\lceil \frac{T_{trans}}{Y/c} \right\rceil + 1$$

$$t_{trunc} = t_{trans} - (n_{TBF}-1)T + i\Delta t, \quad i = 0,1,2,...$$
$$\tau_{trunc} = t_{trunc} - \frac{\eta}{c}\hat{u}^{inc}\cdot\left(x\hat{x}+y\hat{y}\right). \quad \text{(20b)}$$

Like the 1D case, we note in (20b) that the truncated time vector for the Floquet-part has samples with $\Delta t < T$ for accurate numerical convolution. We also note that to have the correct value at $t = T_{trans}$ after convolution with $g(t)$, the Floquet-series has to be computed from $(n_{TBF}-1)T$ seconds before $t = T_{trans}$, where n_{TBF} is related to the temporal support of the $g(t)$; assumed to be $\left[-T, (n_{TBF}-1)T\right]$. As the final TDGF is required at samples that are T seconds apart, the Floquet-wave part of (20a) has to be properly trimmed at the beginning and down-sampled by N_b, before the two parts are appended. All other parameters, including P and Q are treated as before.

It remains to choose a proper value for T_{trans}. It is shown in [7] that the Floquet-modes inefficiency appears at times on the order of the width of the TBF pulse after t_0. We set $T_{trans} = t_0(x,y,z) + n_{trans}T$ with $n_{trans} = 10$ as a typical value. Further remarks on accelerating the computation of (20) and a numerical example will elucidate these points.

B. Practical aspects and Numerical verification

It becomes evident in the computer implementation of (20a) that the evaluation of the special function $J_0(\cdot)$ can be highly time-consuming. This computational cost can be mitigated in the formula (20a) because by virtue of the third property in (20b), the argument of the Bessel function is guaranteed to be real for all $t > t_{trans}$. Therefore, in addition to using real arithmetic, the Bessel function itself can be obtained by 1D linear interpolation on a table of Bessel function values for real samples which needs to be calculated only once. The Heaviside function in (19) is no more necessary and is removed in (20), because it always equals unity for all $t > t_{trans}$. Furthermore, for the B-Spline family of temporal basis functions, the accelerated convolution method based on moving averages can be used as with the 1D periodic case. However, its contribution to efficiency will be relatively small

here, as the main computational cost for the 2D periodic case now arises from the evaluation of the 2D Floquet modes (their total number being typically one order of magnitude higher than the 1D case) prior to convolution, which dominates over the cost of convolutions.

In Fig. 12 we show the TDGF for a close-to-source observation point; $x = y = 0.0025m, z = 0$ in an array with $X = Y = 1m$ and $\eta = 0$. The time step is defined as $T = 0.1X / c_0$. For Floquet series, P=Q=10 is used and the Floquet modes are obtained at a higher resolution for numerical convolution with the TBF, determined by $\Delta t = 0.1\min\left(T, 2\pi / \omega_{FW\max}\right)$. The TBF is the QBspline function. It is seen that the proximity-improved formula (20) is exact at both early and late times.

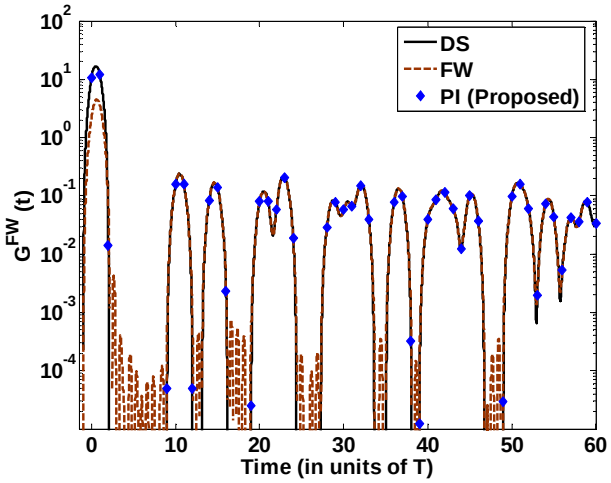

Fig. 12. An example of the near-to-source observation point $x = y = 0.0025, z = 0$ in a 2D periodic array with $X = Y = 1$ and $\eta = 0$. The point of transition corresponds to 42T. the proximity improved (PI) method (20) is exact at both early and late times.

To show the efficiency of the above-mentioned techniques, in Fig. 13 we perform a comparison between the computational efficiencies of direct summation, conventional Floquet-series with direct convolution but with either direct evaluation of Bessel functions or their interpolation, and the proximity-improved method of (5) implemented with the above-mentioned computational techniques, i.e. interpolation for Evaluation of Bessel functions and MA-based convolutions. Because at least O(N_{sim}^2) elements have to be summed for each of the time samples up to T_{sim}, the computational cost of direct summation scales with $O(N_{sim}^3)$. The Floquet-series methods and the Proximity-improved formula have computational times of $O(N_{sim})$. It can be also seen that the main cost is determined by how the computation of the modes, and in particular the Bessel function, is done. The proposed, proximity-improved method is seen to have a computation time as low as, or better than both DS and the conventional Floquet-series.

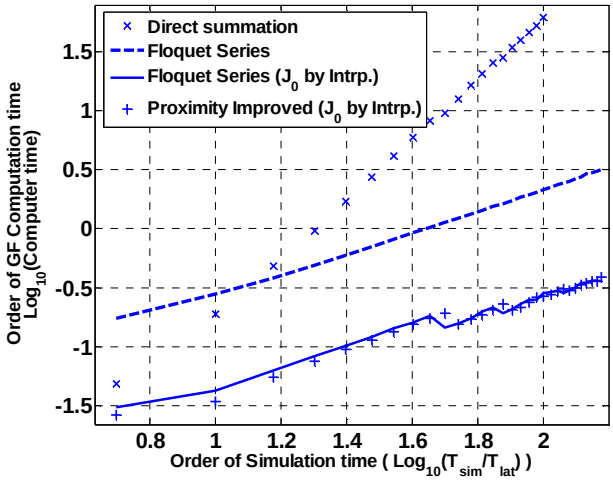

Fig. 13. Comparison of the computation times for the proposed method with several other approaches.

VI. CONCLUSION

We have presented solutions to some of the practical computational challenges of time domain GFs with regard to their implementation in TDIE solvers. It has been shown that for the B-spline basis functions the cost of numerical convolution with basis functions can be reduced by employing an iterative Moving average scheme. Furthermore the inefficiency and the need for higher order modes in the Floquet-series when the observation point approaches a source point is addressed for both the 1D and 2D periodic TDGFs. For the 1D periodic case the problem has been solved by spatially separating the sources adjacent to the unit-interval and treating the remaining sources by the Floquet modes of truncated, semi-inifinite arrays. For the 2D periodic case, we temporally separate the computation of the GF into early and late times, and treat the early times efficiently by direct summation. Several computational

techniques were introduced to accelerate the computation of the obtained results. Together, the contributions presented in this paper can provide for more robust and efficient computation of TDGFs, needed in filling the TDIE coefficients matrices, at both early and late times.

ACKNOWLEDGMENT

M. Saviz thanks Prof. Dr. M. Clemens, Director of the Chair of Electromagnetic Theory, University of Wuppertal for facilitating this research. This work has been partially supported by the Iran Telecommunication Research Center (ITRC) through a research grant.

REFERENCES

[1] A. B. Ali, E. A. Hajlaoui, A. Gharsallah, "Efficient Analysis Technique for Modeling Periodic Structures based on Finite Element Method using High-order Multiscalets Functions," *Applied Computational Electromagnetics Society (ACES) Journal*, vol. 25, no. 9, pp. 755-763, Sept. 2010.

[2] C. Craeye, D. G.-Ovejero, X. Dardenne, "Efficient Numerical Analysis of Arrays of Identical Elements with Complex Shapes" *Applied Computational Electromagnetics Society (ACES) Journal*, vol. 24, no. 2, pp. 224-232, Apr. 2009.

[3] L. E. R. Petersson and J. M. Jin, "A Three-dimensional Time-domain Finite-element Formulation for Periodic Structures," *IEEE Trans. on Antennas Propagat.*, vol. 54, no. 1, pp. 1656-1666, Jan. 2006.

[4] L. E. R. Petersson and J. M. Jin, "A Two-dimensional Time-domain Finite-element Formulation for Periodic Structures," *IEEE Trans. on Antennas Propagat.*, vol. 53, no. 4, pp. 1480-1488, Apr. 2005.

[5] G. Valerio, P. Baccarelli, P. Burghignoli and A. Galli, "Comparative Analysis of Acceleration Techniques for 2-D and 3-D Green's Functions in Periodic Structures Along One and Two Directions," *IEEE Trans. Antennas Propagat.*, vol. 55, pp. 1630, 2007.

[6] A. Cucini, S. Maci, "Macro-Scale Basis Functions for the Method of Moment Analysis of Large Periodic Microstrip Arrays," Applied *Computational Electromagnetics Society (ACES) Journal*, vol. 21, no. 3, pp. 256-266, November 2006.

[7] N-W. Chen, M. Lu, F. Capolino, B. Shanker and E. Michielssen, "Floquet-wave-based Analysis of Transient Scattering from Doubly Periodic Discretely Planar, Perfectly Conducting Structures," *Radio Sci.*, vol. 40, RS4007, 2005.

[8] L.B. Felsen and F. Capolino, "Time Domain Green's Function for an Infinite Sequentially Excited Periodic Line Array of Diploes," *IEEE Trans. Antennas Propagat.*, vol. 48, no. 6, pp. 921-931, Jun. 2000.

[9] F. Capolino and L.B. Felsen, "Frequency and Time Domain Green's Functions for a Phased Semi-Infinite Periodic Line Array of Dipoles," *IEEE Trans. Antennas Propagat.*, vol. 50, no. 1, pp. 31-41, Jan. 2002.

[10] F. Capolino and L.B. Felsen, "Time Domain Green's Functions for an Infinite Sequentially Excited Periodic Planar Array of Dipoles," *IEEE Trans. Antennas Propagat.*, vol. 51, no. 2, pp. 160-170, Feb. 2003.

[11] F. Capolino and L.B. Felsen, "Frequency and Time Domain Green's Functions for a Phased Semi-Infinite Periodic Line Array of Dipoles," *IEEE Trans. Antennas Propagat.*, vol. 50, no. 1, pp. 31-41, Jan. 2002.

[12] J. Gao and B. Shanker, "Time Domain Weyl's Identity and the Causality Trick Based Formulation of the Time Domain Periodic Green's Function," *IEEE Trans. on Antennas Propagat.*, vol. 55, no. 6, pp. 1656-1666, 2007.

[13] P. Wang, M. Y. Xia, J. M. Jin, L. Z. Zhou, "Time-domain Integral Equation Solvers using Quadratic B-spline Temporal Basis Functions," *Microwave and Optical Technology Letters*, vol. 49, Issue 5, pp. 1154-1159, May 2007.

[14] M.Y. Xia, G.H. Zhang, G.L. Dai and C. H. Chan, "Stable Solution of Time Domain Integral Equation Methods using Quadratic B-Spline Temporal Basis Functions," *Journal of Computational Mathematics*, vol. 25, no. 3, pp. 374-384, 2007.

[15] M. Ghaffari-Miab, Z. H. Firouzeh, R. Faraji-Dana, R. Moini, S. H. H. Sadeghi, and G. A. E. Vandenbosch, "Time-domain MoM for the Analysis of Thin-wire Structures above Half-space Media using Complex-time Green's Functions and Band-limited Quadratic B-spline Temporal Basis Functions," *Engineering Analysis with Boundary Elements*, vol. 36, pp. 1116-1124, 2012.

[16] M.J. McDonnell, "Box-Filtering Techniques," *Computer Graphics Image Processing*, vol. 17, pp. 65-70, 1981.

[17] A. V. Oppenheim and R.W. Schafer, *Discrete-Time Signal Processing*, *Third Edition*. Upper Saddle River, NJ: Prentice-Hall Inc., 2009.

Mehrdad Saviz received his B.Sc. from the Iran University of Science and Technology, in 2005 and the M.Sc. degree from the University of Tehran, in 2007, where he is currently a Ph.D. Candidate. His research interests include computational electromagnetics, periodic electromagnetic structures, and numerical microwave dosimetry.

Reza Faraji-Dana received the B.Sc. degree (with honors) from the University of Tehran, Tehran, Iran, in 1986 and the M.Sc. and Ph.D. degrees from the University of Waterloo, Waterloo, ON, Canada, in 1989 and 1993, respectively, all in electrical engineering. He was a Postdoctoral Fellow with the University of Waterloo for one year. In 1994, he joined the School of Electrical and Computer Engineering, University of Tehran, where he is currently a professor.

He has been engaged in several academic and executive responsibilities, among which was his deanship of the faculty of Engineering for more than four years, up until summer 2002, when he was elected as the University President by the university council. He was the President of the University of Tehran until December 2005. He is the author of several technical papers published in reputable international journals and refereed conference proceedings and received the Institution of Electrical Engineers Marconi Premium Award in 1995. He was the Chairman of the IEEE-Iran Section from 2007 until 2009. Prof. Faraji-Dana is an associate member of the Iran Academy of Sciences.